Lead Telluride *p-n* Junctions for Infrared Detection: Electrical and Optical Characteristics

A. S. Barros, E. Abramof, and P. H. O. Rappl

Laboratório Associado de Sensores e Materiais, Instituto Nacional de Pesquisas Espaciais,
Caixa Postal 515, 12245-970 São José dos Campos-SP, Brazil

PbTe mesa diodes were fabricated from a series of $p-n$ junctions grown on BaF_2 substrates. For this series, the hole concentration was kept constant at 10^{17} cm^{-3} and the electron concentration varied between 10^{17} and 10^{19} cm^{-3}. Capacitance versus voltage analysis revealed that for $n > 10^{18}$ cm^{-3}, a one-sided abrupt junction is formed. The direct and reverse branches of the current versus voltage curves exhibited different forms among the diodes. The R_0A product varied between 0.23 and 31.8 Ωcm^2, and the integral detectivity ranged from 1.1×10^8 to 6.5×10^{10} cmHz$^{1/2}$W^{-1}. The performance of the best PbTe photodiodes fabricated here is comparable to the commercial InSb and HgCdTe infrared detectors, and to the PbTe sensors grown on Si substrate.

I. INTRODUCTION

Due to its energy gap of 190 meV at 77K, lead telluride is a good candidate material for detection applications in the mid-wavelength infrared region. PbTe photovoltaic infrared sensors can be either of the Schottky barrier [1] or of $p-n$ junction types [2,3]. The photodiodes are normally made from PbTe layers grown on BaF_2 substrates or on Si substrates using fluoride buffer layers. With device performance comparable to the metal Schottky barriers, PbTe $p-n$ junctions have recently attracted attention as infrared sensors [3-5]. It is well known that the electrical characteristics of the *p-n* junction strongly influence the detector performance.

In this work, we decided to investigate the electrical and optical characteristics of PbTe $p-n$ junctions as a function of the carrier concentration of the constituent layers. For this purpose, we grew a series of PbTe $p-n$ junctions by molecular beam epitaxy (MBE) on (111) BaF_2 substrates. For this series, the hole concentration of the PbTe *p*-layer was kept constant at 10^{17} cm^{-3} and the electron concentration of the *n*-type layer was varied between 10^{17} and 10^{19} cm^{-3}. Mesa diodes were fabricated by lithography process and assembled in a LN$_2$ cryostat for characterization.

Capacitance versus voltage (CxV) and current versus voltage (IxV) characteristic curves were measured for diodes produced from the different $p-n$ junctions. We also measured the integral detectivity and spectral response, in an infrared optical bench. It was possible to correlate the device's figures of merit to the data obtained from the electrical characterization.

II. DEVICE FABRICATION

All samples were grown in a Riber 32P MBE apparatus equipped with effusion cells containing PbTe, Te and Bi_2Te_3 solid sources. Before properly growing the $p-n$ junctions, PbTe reference layers were grown on BaF_2 substrates in order to determine the best MBE growth parameters to obtain both types of conduction. The resistivity, type and carrier concentration, and mobility of the reference layers were measured at 300 and 77K in a Hall Effect system in automatic data acquisition mode with an electromagnet field of 0.7 Tesla.

Since the deviation from stoichiometry plays an important role in the carrier character of the lead salts, our MBE $Pb_{1-y}Te_y$ solid source is intentionally prepared metal rich (y=0.495). Using this source, an *n*-type PbTe layer with an electron concentration of about 5×10^{16}cm^{-3} is normally grown at the usual substrate temperature of 30°C without additional Te flux. In order to obtain the *p*-type layer, the additional Te flux is increased until the character transition from *n* to *p* occurs, as shown in Fig. 1. An extra Te flux of about 8×10^{-9} Torr is necessary in these conditions to change the carrier type.

By playing with the stoichiometry in the MBE system, both *p* and *n*-type PbTe layers with carrier concentration in the range of 10^{17}cm^{-3} could be obtained. To achieve higher electron concentration, the PbTe layers must be doped extrinsically. Bismuth, through the Bi_2Te_3 effusion cell, is normally used as an *n*-type dopant. A detailed study of Bi doping of PbTe layers in our MBE system was previously done [6]. Using this work as a reference, we have determined the Bi_2Te_3 flux necessary to grow PbTe layers with the desired electron concentration of 10^{17}, 10^{18} and 10^{19} cm^{-3}.

After this calibration procedure, a series of $p-n$ junction samples were produced. To form the junctions, a 5 μm thick *p*-type layer is firstly grown on top of a BaF_2 substrate followed by an *n*-type layer of approximately 2 μm. For identification, the junctions with electron concentration in order of 10^{17}, 10^{18} and 10^{19} cm^{-3} were named $p-n$, $p-n^+$ and $p-n^{++}$, respectively.

Mesa structures were fabricated by lithography process. A stainless steel mask with circular holes with diameters of 1.0 and 0.3 mm was used to deposit Au discs with 200 nm of thickness on top of the *n*-type layer. An electron beam source was used to evaporate gold and a quartz crystal monitor controlled the film thickness. These discs were used as protective masks for the etching process as well as metallic contacts. Mesas were etched using a solution of Br_2:HBr:H_2O
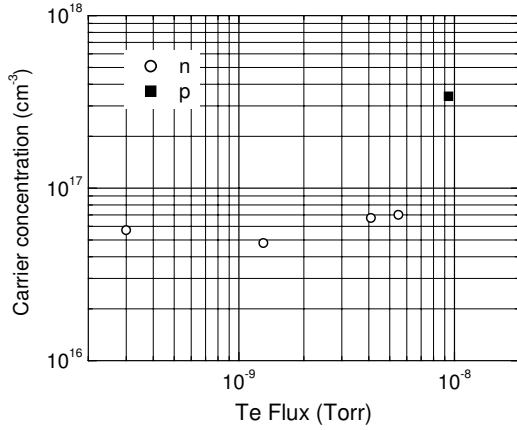
FIG. 1: Carrier concentration at 77 K versus additional Te flux for the PbTe layers grown at 300^oC. The transition of character n to p occurs at about 8×10^{-9} Torr.

(1:40:40) until the p-type layer is reached. Another stainless steel mask was used to deposit Au pads involving each mesa structure to form the diode. Each 15×15 mm^2 BaF$_2$ wafer contain nine diodes with the two different mesa diameters. Gold wires were soldered to both Au pads with indium. The diode was mounted on a Cu plate and assembled in a LN$_2$ cryostat.

III.   C×V CHARACTERISTICS

The capacitance versus voltage characteristic of the produced diodes was measured with a HP4280A capacitance meter. The capacitance is measured through an alternate signal of 10 or 30 mV in a frequency of 1MHz applied together with the DC voltage. The maximum capacitance measurable in this equipment is 2nF. Due to the high dielectric constant of PbTe (κ= 800 @ 77K), the diodes with 0.3 mm of diameter were designed in order to not overpass this value.

The upper panel of Fig. 2 shows the CxV characteristic at 80K of a diode fabricated from a $p - n$ PbTe junction (p and $n \sim 10^{17}$ cm^{-3}), and the lower panel plots the inverse of square of the specific capacitance C$_e$ (capacitance per unit area) as a function of the reverse voltage. The complete non linear behavior of the $1/C_e^2$xV curve, observed for this diode, indicates that the depletion region extends to both sides of the junction. In the other hand, for the p-n^+ and p-n^{++} junctions, the $1/C_e^2$xV plot exhibited an almost linear behavior, as shown in the lower panel of Fig. 3. This result indicates that for electron concentration higher than 10^{18} cm^{-3}, a one-sided abrupt PbTe junction is formed with the depletion region located practically at the p side. For this type of junction, the hole concentration can be determined by the slope of the $1/C_e^2$xV plot and the depletion width can be obtained from the CxV characteristic [5].

The hole concentration determined from the CxV characteristic of the diodes fabricated from the $p - n^+$ junction was 1.1×10^{17} cm^{-3}, a value very close to $p = 1.8 \times 10^{17}$cm^{-3} obtained for the reference layer by Hall Effect measurement.
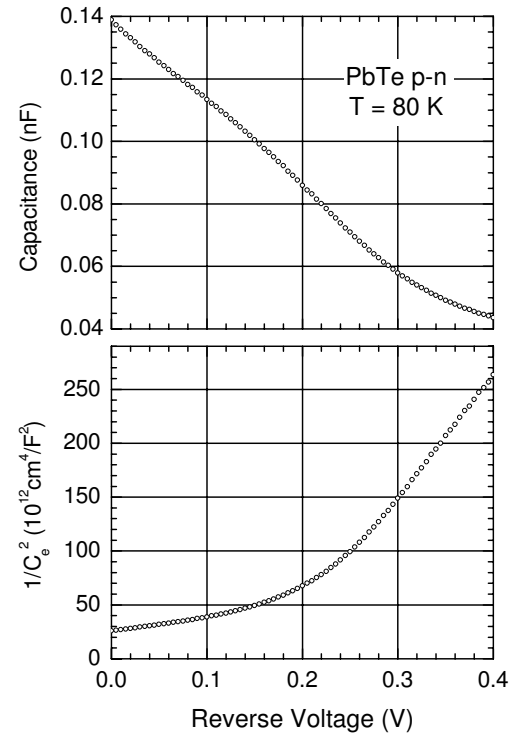

FIG. 2: CxV and $1/C_e^2$xV curves, where C$_e$ is the capacitance per unit area, for a $p - n$ PbTe junction ($p = n \sim 10^{17}$ cm^{-3}).
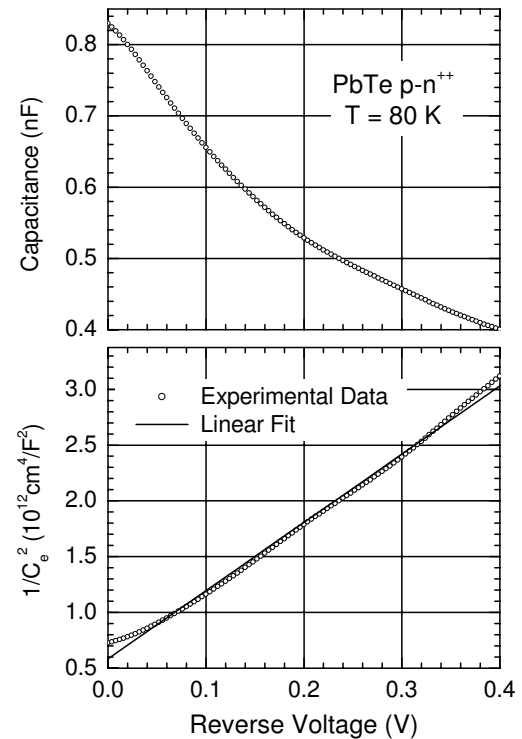

FIG. 3: CxV and $1/C_e^2$xV plots for a $p - n^{++}$ PbTe junction (p=10^{17} and n= 10^{19}cm^{-3}).

In case of diodes from the $p - n^{++}$ junctions, a lower value of hole concentration at about 3×10^{16} cm^{-3} was determined from the slope of the $1/C_e^2 \times V$ plot (Fig. 3). This fact indicate that bismuth inter-diffusion may start to take place for PbTe junctions with electron concentration as high as 10^{19} cm^{-3}. The depletion width for the $p - n^+$ and $p - n^{++}$ junctions at V=0 were close to 1 μm. This value agrees with published data for PbTe $p - n^+$ diodes grown on Si substrates [3].

IV. IXV CHARACTERISTICS

The current versus voltage characteristics of all diodes were measured in a self-assembled automatic system composed of a programmable power supply, an ammeter and a voltmeter [5]. Fig. 4 shows, as an example, the IxV curve for a PbTe diode fabricated from $p - n^{++}$ junction. In this case, the diode presented a nice IxV characteristic with a low leakage current in the reverse branch and a small series resistance in the forward direction. The lower panel of Fig. 4 plots the inverse of the derivative of the IxV curve ($\delta V/\delta I$). This plot allows the determination of the incremental differential resistance (R$_0$) and the R$_0$A product, where A is the photodiode area.
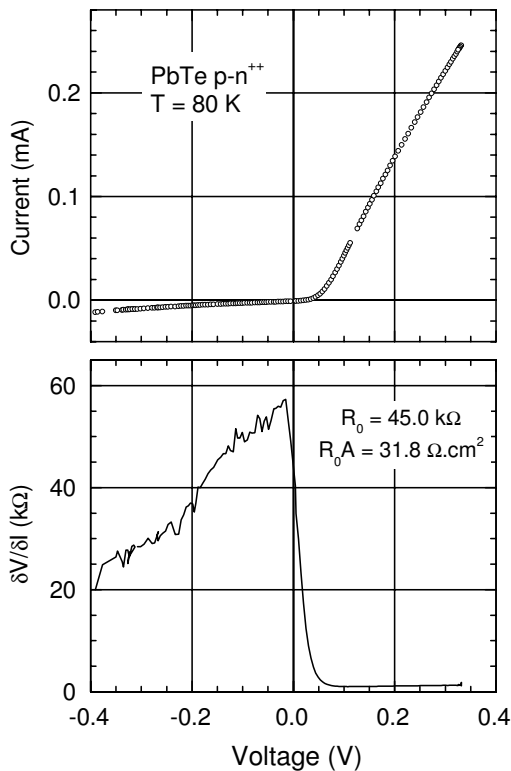

FIG. 5: IxV characteristic for a PbTe diode presenting a large leakage produced from a $p - n^{++}$ junction.

FIG. 4: IxV characteristic for a diode with a small leakage current fabricated from a p-n^{++} PbTe junction.

We have observed, contrarily to the CxV results, that the IxV curves exhibited different formats and values among all measured diodes. Even for diodes fabricated from the same junction, different shapes were observed for both direct and
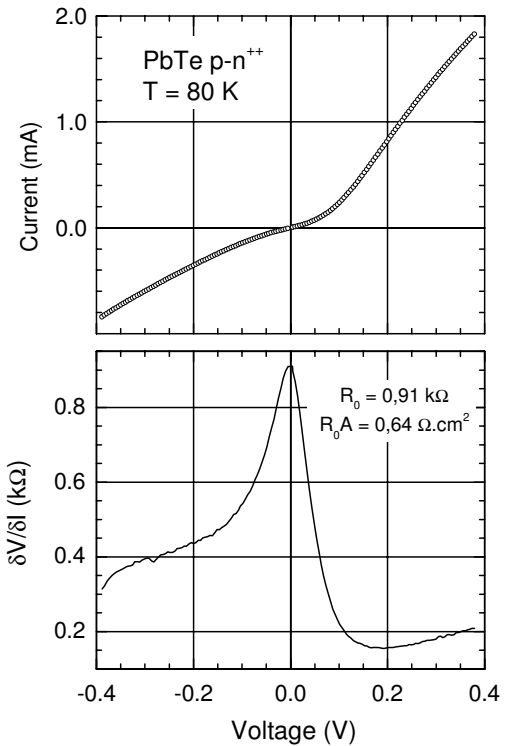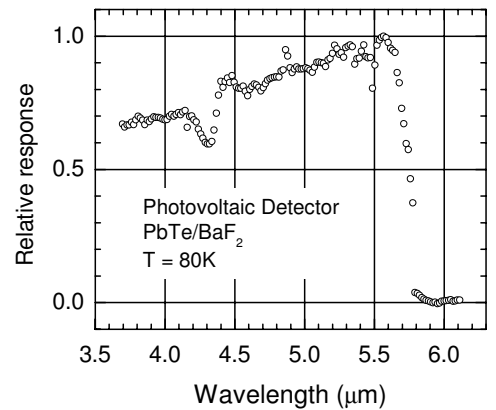

FIG. 6: Typical spectral response of PbTe photodiodes fabricated here.

reverse branches. The leakage current and the series resistance presented a significant variation among the diodes. Fig. 5 shows, as an illustration, the IxV curve of a diode, which exhibits a large leakage current, produced from a $p - n^{++}$ junction.

The incremental differential resistance, determined for all diodes, varied between 0.32 and 45 kΩ and the R$_0$A product

from 0.23 to 31.8 Ωcm^2. Due to this variation, it was not possible to find any correlation between the parameters obtained from the IxV curves and the electron concentration in the $p-n$ junction. We believe that this large variation observed for the IxV curves in the different diodes is due to non-uniformities during the diode processing and the absence of a passivation layer.

V. DETECTIVITY AND SPECTRAL RESPONSE

The photodiodes' figures of merit, i.e. detectivity and spectral response, were characterized in an infrared optical bench. The integral detectivity D* was measured for all PbTe photodiodes at 80K. The radiation from a blackbody source at T = 900 K, chopped with a frequency of 900 Hz, illuminates the detector through the BaF_2 window of the cryostat. A power density of 5.65 x 10^{-4} Wcm^{-2} reaches the detector and the root mean square voltage signal is measured in a lock-in amplifier with a bandwidth of 14 Hz. The detector noise was measured for a background at 300K and a field-of-view of 30°. The detectivity values of all measured photodiodes varied from $1.1x10^8$ to $6.5x10^{10}$ $cmHz^{1/2}W^{-1}$. Like the IxV curves, the detectivity also showed a large fluctuation among the different diodes. The detectivity D* correlated well with the R_0A product. Diodes with the highest R_0A values exhibit the best performance in infrared detection, as expected.

The highest values of R_0A product, measured for the PbTe photodetectors grown on BaF_2 substrates during this work, are close to the values found in the literature for PbTe $p-n$ junction infrared sensor grown on Si substrates [3,4]. It is important to mention that the performance of the best PbTe photodiodes fabricated here with integral detectivity D* of 6 x 10^{10} $cmHz^{1/2}W^{-1}$ is comparable to commercial InSb and HgCdTe infrared detectors with cut-off wavelength around 6 μm that show peak detectivity $D^*(\lambda_p)$ in the range of 10^{11} $cmHz^{1/2}W^{-1}$ at 77K [7].

The spectral response was measured in the same system as for the detectivity, by placing a grating monochromator between the infrared source (Glowbar) and the detector. The spectral response of the infrared sensor under test is compared to the response of a piroeletctric reference detector. Fig. 6 shows a typical spectral response of the photodiode, which exhibits the cutoff wavelength of 5.9 μm, corresponding to the energy gap of PbTe. The drop in response observed at 4.3 μm, in the region of CO_2 absorption, is due to the difference in optical path for the measured photodiode and the piroelectric detector.

VI. CONCLUSION

We have determined the electrical and optical properties of PbTe mesa diodes fabricated from $p-n$ junctions with different electron concentrations. The CxV analysis revealed a one-sided abrupt junction for n > 10^{18} cm^{-3} with depletion widths around 1 μm. The p concentration determined from the slope of $1/C_\ell^2 xV$ plot agreed with the one obtained from Hall measurements. The IxV curves exhibited different formats for both direct and reverse branches. The leakage current, the series resistance and the D* values presented a significant variation among the different diodes. The detectivity correlated well with the R_0A product, and D* values close to $10^{11} cmHz^{1/2}W^{-1}$ were measured for the best photodiodes produced here.

[1] H. Zogg, A. Fach, C. Maissen, J. Masek, and S. Blunier, Optical Engineering **33**, 1440 (1994).

[2] C. Boschetti, P.H.O Rappl, A.Y. Ueta, I.N. Bandeira, Infrared Phys. **34**, 281 (1993).

[3] J. John and H. Zogg, J. Appl. Phys. **85**, 3364 (1999).

[4] D. Zimin, K. Alchalabi, and H. Zogg, Physica E **13**, 1220 (2002).

[5] A.S. Barros, E. Abramof, P.H.O. Rappl, A.Y. Ueta, and H. Closs, Braz. J. Phys. **34**, 641 (2004).

[6] A.M.P. Anjos, E. Abramof, P.H.O. Rappl, A.Y. Ueta, and H. Closs, Braz. J. Phys. **34**, 653 (2004).

[7] A. Rogaslki, Infrared Phys. & Tech. 43, 187 (2002).